

MRS Advances © 2020 Materials Research Society. This is an Open Access article, distributed under the terms of the Creative Commons Attribution-NonCommercial-NoDerivatives licence (<http://creativecommons.org/licenses/by-nc-nd/4.0/>), which permits non-commercial re-use, distribution, and reproduction in any medium, provided the original work is unaltered and is properly cited. The written permission of Cambridge University Press must be obtained for commercial re-use or in order to create a derivative work.
DOI: 10.1557/adv.2020.259



Sodium Induced Morphological Changes of Carbon Coated TiO₂ Anatase Nanoparticles – High-Performance Materials for Na-Ion Batteries

G. Greco¹, S. Passerini^{2,3}

¹ Helmholtz-Zentrum Berlin für Materialien und Energie Gmb (HZB), Hahn-Meitner-Platz 1, D-14109 Berlin, Germany;

² Helmholtz Institute Ulm (HIU), Helmholtzstr. 11, 8901 Ulm, Germany,

³ Karlsruhe Institute of Technology (KIT), P.O. Box 3640, 76021 Karlsruhe, Germany.

Abstract

The most promising candidate as an everyday alternative to lithium-ion batteries (LIBs) are sodium-ion batteries (NIBs). This is not only due to Na abundance, but also because the main principles and cell structure are very similar to LIBs. Due to these benefits, NIBs are expected to be used in applications related to large-scale energy storage systems and other applications not requiring top-performance in terms of volumetric capacity. One important issue that has hindered the large scale application of NIBs is the anode material. Graphite and silicon, which have been widely applied as anodes in NIBs, do not show great performance. Hard carbons look very promising in terms of their abundance and low cost, but they tend to suffer from instability, in particular over the long term. In this work we explore a carbon-coated TiO₂ nanoparticle system that looks very promising in terms of stability, abundance, low-cost, and most importantly that safety of the cell, since it does not suffer from potential sodium plating during cycling. Maintaining a nano-size and consistent morphology of the active material is a crucial parameter for maintaining a well-functioning cell upon cycling. In this work we applied Anomalous

Small Angle X-Ray Scattering (ASAXS) for the first time at the Ti K-edge of TiO₂ anatase nanoparticles on different cycled composite electrodes in order to have a complete morphological overview of the modifications induced by sodiation and desodiation. This work also demonstrates for the first time that the nanosize of the TiO₂ is maintained upon cycling, which is in agreement with the electrochemical stability.

INTRODUCTION

Lithium-ion batteries (LIBs) are the power source of choice for portable electronic devices and for hybrid and fully electric vehicles.^{1–3} However, the use of lithium as the main power source for electromobility and stationary applications is questionable due to limited global lithium resources and sustainability in terms of the harmful elements of their constituents.⁴ Several “beyond lithium” technologies with more sustainable chemistries are currently being investigated, including potassium ion batteries (PIBs), magnesium ion batteries (MIBs), and sodium ion batteries (NIBs), but NIBs are closest to commercialization for several reasons.^{5–8} One is the abundance of sodium in both seawater and the Earth’s crust, which offers practically unlimited overall availability. Additionally, NIBs and LIBs share the same working principles and cell structures, thus Na cells will benefit from previously developed battery cell-manufacturing technologies.⁹ However, for this system appropriate anode materials are still needed. Hard carbons look like a very promising candidate for anode in NIBs,¹⁰ but they suffer from safety concerns due to a long plateau in the voltage profile which is very close to the Na metal plating potential.^{11,12} Moreover, graphite has been investigated as an anode material for NIBs, but it shows poor performance in terms of capacity.^{13–15} Among all the suitable low-cost and abundant candidates, TiO₂ anatase nanoparticles have shown some of the most intriguing performance characteristics in terms of stability alongside the fact that it does not suffer from the risk of sodium plating upon cycling.^{16,17,18} It has been demonstrated that particle size and carbon coating strongly control the electrochemical performance of TiO₂ in NIBs.¹⁹ The carbon coated TiO₂ nanomaterials synthesized by Tahir, *et al.*¹⁹ show extraordinary performance in terms of specific capacity (up to 227 mAh g⁻¹), rate capability, stability, and efficiency (≈99.8%). In our previous work, the electrochemical mechanism of Na⁺ ion insertion in this high-performance material was successfully followed. In this work we demonstrate that the Na⁺ insertion in TiO₂ occurs after an initial activation and structural amorphization, which result in electronic and atomic structural rearrangements in tandem with the electrochemical behavior of the active material.²⁰ For completeness, in this work we apply a particular property of the Small Angle Scattering (SAXS) technique, such as the Anomalous SAXS (ASAXS) one in order to directly probe changes in the TiO₂ nanoparticle size during the sodiation/desodiation cycle. Particle aggregation and Ostwald ripening²¹ are phenomena commonly observed in solid solutions, and represent pathways that can strongly decrease the electrochemical performance of a cell comprised of nanocrystalline materials. In this work, we use ASAXS to investigate the effect of the sodiation and desodiation process on the TiO₂ the particle’s size.

Anomalous Small Angle X-ray Scattering: Theory

Small Angle X-Ray Scattering (SAXS) is a well-known and powerful method for the characterization of nano-sized objects below ~1 nm and up to ~100 nm, and which is independent of the atomic structure of the system. SAXS cannot only be used to

determine size but also information related to the size distribution and morphology of the nanostructures. However, in the case of multi-component systems it can be difficult to distinguish the contribution to the SAXS signal arising from the matrix from that of the nanoparticles, which consequently complicates data evaluation.^{22–24} An electrode is a good example of this case, as they are composed of different constituents including a conductive matrix, the active nanomaterial, and a binder, all of which contribute to the total SAXS signal. Anomalous SAXS (ASAXS) gives the possibility to distinguish the scattering contributions arising from different atomic elements and separating these contributions. This technique is based on the energy dependence of the atomic scattering factors of an element. The scattering factor shows a strong energy dependent response close to the absorption edge of an element relative to that far from the edge (equal to the electron number of such element Z). This energy dependence influences the intensity of the total scattering curve so that far from the edge of an element the intensity is higher than close to the edge, highlighting in which q range such element is distributed. In fact, in general, the atomic scattering factor, $f(E)$, can be written as:

$$f(E) = f_0 + f'(E) + if''(E) \quad (1)$$

where $f_0 + f'(E)$ is the real part and $f''(E)$ the imaginary part of the atomic scattering factors. The anomalous dispersion corrections, $f'(E)$ and $f''(E)$ are energy dependent and give information related to the contrast of a given element, in particular near an absorption edge. The dispersion corrections are related to each other by the well-known Kramers–Kronig relation. The total scattering intensity, $I(q, E)$, is a function of the X-ray energy and of the magnitude of the momentum transfer $q = \left(\frac{4\pi}{\lambda}\right) \sin\left(\frac{\theta}{2}\right)$, where λ is the X-ray wavelength and θ is the scattering angle. It can be written including the anomalous contributions as:

$$I(q, E) = f_0 I_0(q) + 2 f_0 f'(E) I_{0R}(q) + [f'^2(E) + f''^2(E)] I_R(q) \quad (2)$$

This equation is also known as the Stuhrmann equation,²³ and consists of three components: the energy-independent normal SAXS term $I_0(q)$, the scattering cross term $I_{0R}(q)$ and the pure resonant scattering, $I_R(q)$. This resonant scattering term contains information about the spatial distribution of the resonant chemical element distributed in nanosized structures only. To solve the equation, $I(q, E)$, and obtain the resonant scattering term, $I_R(q)$, scattering measurements must be performed at a minimum of three different energies.²⁴

Anomalous Small Angle X-ray Scattering: measurements and data analysis

ASAXS measurements were performed at the BESSY II synchrotron radiation facility (HZB, Berlin, Germany) using the four-crystal monochromator (FCM) beamline of the Physikalisch-Technische Bundesanstalt (PTB), the German National Metrology Institute.²⁵ The combination of this beamline and the ASAXS instrument of the HZB²⁶ has already been described.²⁷ The scattering patterns were recorded with a new in-vacuum large-area hybrid pixel detector (Pilatus 1M, Dectris Ltd, Switzerland). As no window is required between the sample and the sensitive modules of this detector, the entire photon energy range of the FCM beamline (from 1.75 to 10 keV) can be used for SAXS and ASAXS measurements. The SAXS measurements were performed at five different energies below the Ti K -edge (4768, 4900, 4944, 4959, 4965 eV), as reported in Figure 1 below. The two-dimensional raw scattering data patterns were collected and reduced as

previously described in the literature.²⁰ XAFS measurements were performed at the Ti *K* absorption edge, shown in our previous work.²⁰ To qualitatively evaluate the resonant contribution of the TiO₂ active material, we evaluate the scattering curves intensity multiplied for the square of the modulus of the scattering vector *q* for all the electrodes. The nanoparticle contribution were finally evaluated to the first approximation using the *SASfit* program²⁸ with a spherical model.

Sample description

The samples investigated are composite electrodes, mostly consisting of carbon coated TiO₂ anatase (labeled as C-TiO₂) nanoparticles synthesized and processed as previously reported.¹⁹ The dry C-TiO₂ electrodes had a composition of 65 wt % TiO₂, 25 wt % carbon, including the carbon present in the C-TiO₂ particles and the conductive agent (Super C65, IMERYS, Switzerland), and 10 wt % binder (polyvinylidene fluoride PVDF, ARKEMA). Uncoated TiO₂ electrode composition was 65 wt % TiO₂, 25 wt % Super C65, and 10 wt % PVDF. Three-electrode cells were assembled in a drybox (H₂O and O₂ content lower than 1 ppm) using the prepared electrodes as the working electrodes. The electrolyte was a 1 M solution of NaClO₄ (98% Sigma-Aldrich) dissolved in a 1:1 mixture (by volume) of ethylene carbonate (UBE) and propylene carbonate (Sigma-Aldrich). Sodium metal (99.8%, ACROS ORGANICS) was used as both the counter and reference electrodes. Thus, all given potentials in this paper refer to the Na/Na⁺ reference couple. Sodiation at each desired level was achieved by applying a constant current to the three-electrode cells to a predefined electrode potential; this potential was then held for at least 1 h to allow equilibration of the electrode bulk. After sodiation to the desired level, the cells were disassembled, and the electrodes were carefully rinsed in dimethyl carbonate (DMC Sigma-Aldrich 99.9%, anhydrous) to remove any residual electrolyte. The sample preparation and cell assembly and disassembly were performed in an Ar-filled glovebox (with oxygen and water concentrations lower than 0.1 ppm) to avoid any reactions with oxygen or moisture. The transfer from the glovebox to the instruments was done using an airtight container. For the *ex-situ* characterization, several cells were assembled and stopped at different degrees of sodiation within the first and second cycles as described in our previous work.²⁰ Four electrodes were investigated, including a pristine sample (S₁), after sodiation at 0.15 V (S₂), desodiation at 2.0 V (S₃), and a fully sodiated sample (S₄).

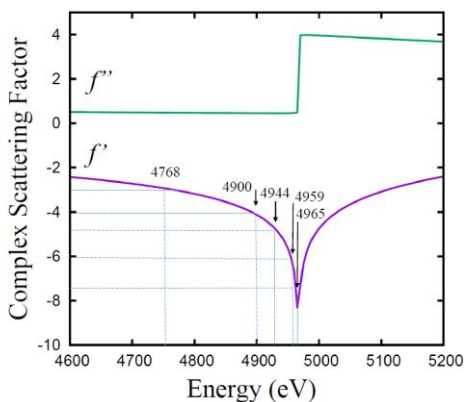


Figure 1: Anomalous dispersion corrections f'' and f' for Ti near the Ti K-edge (4966.4 eV). The five X-ray energies for the SAXS measurements are indicated.

RESULTS AND DISCUSSION

C-TiO₂ composite electrodes: ASAXS and particle size evaluation

Figure 2 shows the SAXS intensities multiplied by the square of modulus of the wave vector q at five different energies for the samples under investigation. In the Figure 2 d the resonant effect represented by different intensities for different energies is highlighted. This effect is due to scattering factors difference closer to the Ti K -edge as describe in the Anomalous Angle X-ray Scattering Theory section, above. This difference is already a fingerprint of the presence of Ti in the q range of the nanoparticles $\sim 0.2 - 2.0 \text{ nm}^{-1}$, or $d = 30 - 3 \text{ nm}$. In fact the resonant effect represent only the scattering contribution that comes from the Ti element in the sample giving an evidence not only to the TiO₂ nanoparticles dimension but also to its distribution in the electrode. In our previous report, we demonstrated that the q range between $0.04 - 0.24 \text{ nm}^{-1}$ of the SAXS curve is related to particle aggregates. We do not observe a resonant effect in this q range after electrode preparation and in particular after the first sodiation (S₂).

The resonant effect of the curves in Figure 2 give a first qualitative evaluation about the Ti distribution in the cycled electrodes. In fact after the first sodiation, at point S₂, we could not be sure about the morphology of the nanoparticles and we could not have a reliable model for fitting.²⁹ For this reason, additional investigations, such as Transmission Electron Microscopy (TEM), are necessary to confirm the nanoparticle morphology. However as a first approximation we could assume that the scattering curves of all the composite electrodes could be modelled as a sum of two contributions: a curve that represent the additives (conductive materials and binder), modelled as standard background³⁰ and a spherical particle model. As an example, in Figure 3 the best fit of the contribution of the nanoparticles for the sample S₄ is reported. The orange curve of Figure 3 is the nanoparticle contribution obtained by subtracting the background from the total scattering curve in magenta. For the investigated electrodes the scattering intensities decrease with $q^{-\alpha}$ with α varies slightly between 3.75 and 3.80, such value is typical of the carbon materials³¹ used as conductive additive.

The fit of the fully pristine electrodes (S_1) shows the nanoparticles are not aggregated and that the average TiO_2 nanoparticle diameter is ~ 9 nm, as confirmed from SAXS analysis of the pure C- TiO_2 in our previous work.²⁰ After the first cycle, the nanoparticle size does not seem to be strongly affected by the sodiation and desodiation process. In Figure 4 the normalized and volume weighted lognormal size distributions of the samples under investigation are reported. The nanoparticle diameters remain between 8 nm in the fully desodiated case (S_3) and ~ 9.5 nm in the fully sodiated (S_4) electrodes.

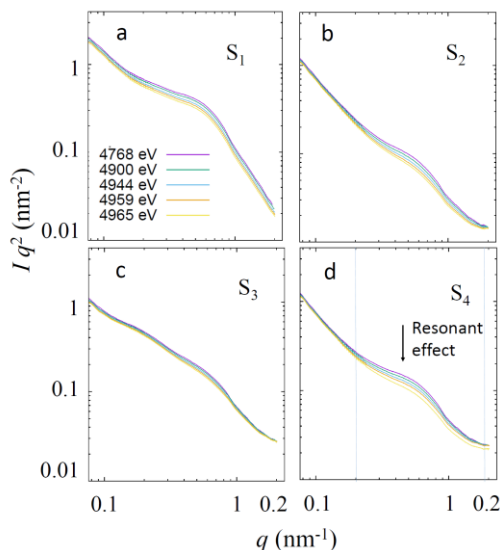


Figure 2: SAXS curves collected at 4768, 4900, 4944, 4959 and 4965 eV (a) S_1 , pristine electrode, (b) S_2 , sodiated at 0.15 V, (c) S_3 desodiated at 2.00 V and (d) S_4 fully sodiated.

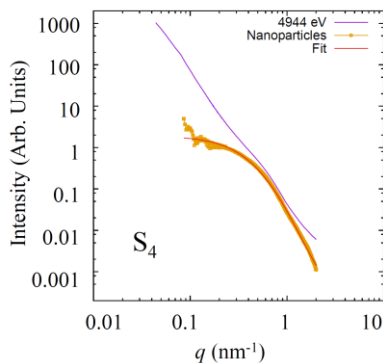


Figure 3: SAXS curves collected at 4944 eV alongside the subtracted curve and their best fits for the electrode S_4 fully sodiated.

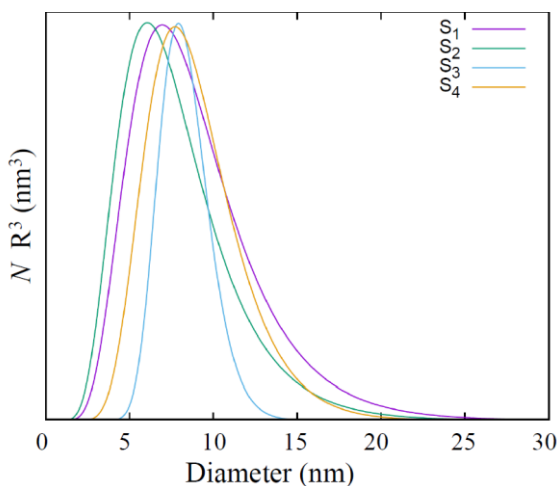


Figure 4: Normalized and Volume weighted lognormal size distributions of the TiO_2 nanoparticles for the various investigated samples.

CONCLUSIONS

Carbon-coated TiO_2 composite electrodes were investigated by ASAXS at different degrees of sodiation during electrochemical cycling, demonstrating that the nanoparticle sizes remain almost unchanged. It was found that after the electrode preparation, the nanoparticles maintain their average diameters, but are no longer aggregated, as shown in our previous work for the pure nanoparticle material.

ACKNOWLEDGMENTS

The authors would like to thank all the PTB group and their support during the data acquisition and Lucien Fumagalli for the helpful help in the SAXS data reduction.

References:

- (1) *High Energy Density Lithium Batteries*; 2010. <https://doi.org/10.1002/9783527630011>.
- (2) Blomgren, G. E. The Development and Future of Lithium Ion Batteries. In *Journal of the Electrochemical Society*; 2017. <https://doi.org/10.1149/2.0251701jes>.
- (3) Notter, D. A.; Gauch, M.; Widmer, R.; Wäger, P.; Stamp, A.; Zah, R.; Althaus, H. J. Contribution of Li-Ion Batteries to the Environmental Impact of Electric Vehicles. *Environ. Sci. Technol.* **2010**. <https://doi.org/10.1021/es903729a>.
- (4) Tarascon, J. M. Is Lithium the New Gold? *Nature Chemistry*. 2010. <https://doi.org/10.1038/nchem.680>.

- (5) Deng, J.; Luo, W.-B.; Chou, S.-L.; Liu, H.-K.; Dou, S.-X. Sodium-Ion Batteries: From Academic Research to Practical Commercialization. *Adv. Energy Mater.* **2018**, *8* (4), 1701428. <https://doi.org/10.1002/aenm.201701428>.
- (6) Pu, X.; Wang, H.; Zhao, D.; Yang, H.; Ai, X.; Cao, S.; Chen, Z.; Cao, Y. Recent Progress in Rechargeable Sodium-Ion Batteries: Toward High-Power Applications. *Small* **2019**, 1805427. <https://doi.org/10.1002/smll.201805427>.
- (7) Roberts, S.; Kendrick, E. The Re-Emergence of Sodium Ion Batteries: Testing, Processing, and Manufacturability. *Nanotechnol. Sci. Appl.* **2018**, *11*, 23–33. <https://doi.org/10.2147/NSA.S146365>.
- (8) Bauer, A.; Song, J.; Vail, S.; Pan, W.; Barker, J.; Lu, Y. The Scale-up and Commercialization of Nonaqueous Na-Ion Battery Technologies. *Adv. Energy Mater.* **2018**, *8* (17), 1702869. <https://doi.org/10.1002/aenm.201702869>.
- (9) Hwang, J. Y.; Myung, S. T.; Sun, Y. K. Sodium-Ion Batteries: Present and Future. *Chemical Society Reviews*. 2017. <https://doi.org/10.1039/c6cs00776g>.
- (10) Dou, X.; Hasa, I.; Saurel, D.; Vaalma, C.; Wu, L.; Buchholz, D.; Bresser, D.; Komaba, S.; Passerini, S. Hard Carbons for Sodium-Ion Batteries: Structure, Analysis, Sustainability, and Electrochemistry. *Mater. Today* **2019**, *23*, 87–104. <https://doi.org/10.1016/J.MATTOD.2018.12.040>.
- (11) Dou, X.; Hasa, I.; Saurel, D.; Jauregui, M.; Buchholz, D.; Rojo, T.; Passerini, S. Impact of the Acid Treatment on Lignocellulosic Biomass Hard Carbon for Sodium-Ion Battery Anodes. *ChemSusChem* **2018**, *11* (18), 3276–3285. <https://doi.org/10.1002/cssc.201801148>.
- (12) Wahid, M.; Puthusseri, D.; Gawli, Y.; Sharma, N.; Ogale, S. Hard Carbons for Sodium-Ion Battery Anodes: Synthetic Strategies, Material Properties, and Storage Mechanisms. *ChemSusChem* **2018**, *11* (3), 506–526. <https://doi.org/10.1002/cssc.201701664>.
- (13) Hasa, I.; Dou, X.; Buchholz, D.; Shao-Horn, Y.; Hassoun, J.; Passerini, S.; Scrosati, B. A Sodium-Ion Battery Exploiting Layered Oxide Cathode, Graphite Anode and Glyme-Based Electrolyte. *J. Power Sources* **2016**, *310*, 26–31. <https://doi.org/10.1016/J.JPOWSOUR.2016.01.082>.
- (14) Dou, X.; Buchholz, D.; Weinberger, M.; Diemant, T.; Kaus, M.; Indris, S.; Behm, R. J.; Wohlfahrt-Mehrens, M.; Passerini, S. Study of the Na Storage Mechanism in Silicon Oxycarbide—Evidence for Reversible Silicon Redox Activity. *Small Methods* **2019**, *3* (4), 1800177. <https://doi.org/10.1002/smt.201800177>.
- (15) Komaba, S.; Matsuura, Y.; Ishikawa, T.; Yabuuchi, N.; Murata, W.; Kuze, S. Redox Reaction of Sn-Polyacrylate Electrodes in Aprotic Na Cell. *Electrochem. commun.* **2012**, *21*, 65–68. <https://doi.org/10.1016/J.ELECOM.2012.05.017>.
- (16) Guo, S.; Yi, J.; Sun, Y.; Zhou, H. Recent Advances in Titanium-Based Electrode Materials for Stationary Sodium-Ion Batteries. *Energy Environ. Sci.* **2016**, *9* (10), 2978–3006. <https://doi.org/10.1039/C6EE01807F>.
- (17) Zhang, W.; Luo, N.; Huang, S.; Wu, N.-L.; Wei, M. Sulfur-Doped Anatase TiO₂ as an Anode for High-Performance Sodium-Ion Batteries. *ACS Appl. Energy Mater.* **2019**, *2* (5), 3791–3797. <https://doi.org/10.1021/acs.aem.9b00471>.
- (18) Xu, Z.-L.; Lim, K.; Park, K.-Y.; Yoon, G.; Seong, W. M.; Kang, K. Engineering Solid Electrolyte Interphase for Pseudocapacitive Anatase TiO₂ Anodes in Sodium-Ion Batteries. *Adv. Funct. Mater.* **2018**, *28* (29), 1802099. <https://doi.org/10.1002/adfm.201802099>.
- (19) Tahir, M. N.; Oschmann, B.; Buchholz, D.; Dou, X.; Lieberwirth, I.; Panthöfer, M.; Tremel, W.; Zentel, R.; Passerini, S. Extraordinary Performance of Carbon-Coated Anatase TiO₂ as Sodium-Ion Anode. *Adv. Energy Mater.* **2016**, *6* (4), 1501489. <https://doi.org/10.1002/aenm.201501489>.
- (20) Greco, G.; A. Mazzi, K.; Dou, X.; Gericke, E.; Wendt, R.; Krumrey, M.; Passerini, S. Structural Study of Carbon-Coated TiO₂ Anatase Nanoparticles as High-Performance Anode Materials for Na-Ion Batteries. *ACS Appl. Energy Mater.* **2019**, *2* (10), 7142–7151. <https://doi.org/10.1021/acs.aem.9b01101>.
- (21) Voorhees, P. W. The Theory of Ostwald Ripening. *J. Stat. Phys.* **1985**. <https://doi.org/10.1007/BF01017860>.
- (22) Greco, G.; A. Mazzi, K.; Dou, X.; Gericke, E.; Wendt, R.; Krumrey, M.; Passerini, S. Structural Study of Carbon-Coated TiO₂ Anatase Nanoparticles as High-Performance Anode Materials for Na-Ion Batteries.

- ACS Appl. Energy Mater.* **2019**, 0 (ja), null-null.
<https://doi.org/10.1021/acsaem.9b01101>.
- (23) Stuhrmann, H. B. Resonance Scattering in Macromolecular Structure Research. In *Characterization of Polymers in the Solid State II: Synchrotron Radiation, X-ray Scattering and Electron Microscopy*; Springer, 1985; pp 123–163.
- (24) Hoell, A.; Tatchev, D.; Haas, S.; Haug, J.; Boesecke, P. On the Determination of Partial Structure Functions in Small-Angle Scattering Exemplified by Al 89 Ni 6 La 5 Alloy. *J. Appl. Crystallogr.* **2009**.
<https://doi.org/10.1107/S0021889808042453>.
- (25) Krumrey, M. Design of a Four-Crystal Monochromator Beamline for Radiometry at BESSY II. *J. Synchrotron Radiat.* **1998**, 5 (1), 6–9.
<https://doi.org/10.1107/S0909049597011825>.
- (26) Hoell, A.; Zizak, I.; Bieder, H.; Mokrani, L. German Patent DE 10 2006 029 449. 2007.
- (27) Meli, F.; Klein, T.; Buhr, E.; Frase, C. G.; Gleber, G.; Krumrey, M.; Duta, A.; Duta, S.; Korpelainen, V.; Bellotti, R.; et al. Traceable Size Determination of Nanoparticles, a Comparison among European Metrology Institutes. *Meas. Sci. Technol.* **2012**.
<https://doi.org/10.1088/0957-0233/23/12/125005>.
- (28) Breßler, I.; Kohlbrecher, J.; Thünemann, A. F. SASfit: A Tool for Small-Angle Scattering Data Analysis Using a Library of Analytical Expressions. *J. Appl. Crystallogr.* **2015**, 48 (5), 1587–1598.
- (29) Haas, S.; Hoell, A.; Würth, R.; Ruessel, C.; Boesecke, P.; Vaimio, U. Analysis of Nanostructure and Nanochemistry by ASAXS: Accessing Phase Composition of Oxyfluoride Glass Ceramics Doped with Er³⁺/Yb³⁺. *Phys. Rev. B* **2010**, 81 (18).
<https://doi.org/10.1103/PhysRevB.81.184207>.
- (30) Tran, H. Y.; Greco, G.; Täubert, C.; Wohlfahrt-Mehrens, M.; Haselrieder, W.; Kwade, A. Influence of Electrode Preparation on the Electrochemical Performance of LiNi_{0.8}Co_{0.15}Al_{0.05}O₂ Composite Electrodes for Lithium-Ion Batteries. *J. Power Sources* **2012**, 210.
<https://doi.org/10.1016/j.jpowsour.2012.03.017>.
- (31) Hoinkis, E. Small-Angle Scattering of Neutrons and x-Rays from Carbons and Graphites. In *Chemistry and physics of carbon vol.25*; Thrower, P. A., Ed.; Marcel Dekker: New York, 1997; pp 71–242.